(Received 13 January 2026, Accepted 3 February 2026, Scheduled 13 February 2026)

Improving Gain-Bandwidth Product of Modified Split Ring Resonators for 6G Wireless Networks

Al-Moatasem Al-Hinaai[1,*], Anthony N. Caruso[1,2], Travis D. Fields[1,2], Mohamed Z. M. Hamdalla[2], and Kalyan C. Durbhakula[2]

[1]School of Science and Engineering, University of Missouri-Kansas City, Kansas City, MO 64110, USA
[2]Missouri Institute for Defense and Energy, University of Missouri-Kansas City, Kansas City, MO 64110, USA

ABSTRACT: Metamaterials are emerging as a key enabler for 6G wireless communications, attracting growing attention from industry due to their engineered electromagnetic properties that enable control over wave propagation. Metamaterials have shown promise across diverse applications; however, the desire to achieve 1 TBPS data rates in 6G communications is partially constrained by a major fundamental challenge in metamaterials: achieving gigahertz of instantaneous bandwidth (IBW) values. To address the IBW issue, we designed, fabricated, and tested a fundamental component of metamaterial, i.e., a modified split ring resonator (MSRR), achieving 90% of the targeted 1 GHz IBW and an effective permeability (μ_{eff}) close to 25 within the IBW. In addition, the gain-bandwidth product (GBWP) is over 1.5× greater than that of commercial 5G antennas, while maintaining the same aperture size of $1.59\lambda_c$. We studied and reported the effect of MSRR frequency-dependent μ_{eff} on the IBW and GBWP and proposed an optimized MSRR design that achieves 3× the bandwidth of a conventional SRR. Finally, we integrated the proposed MSRR atop a wideband patch antenna, enhancing peak realized gain by 6 dBi.

1. INTRODUCTION

The metamaterial industry is projected to grow from USD 0.22 billion in 2024 to USD 1.38 billion by 2029, at a compound annual growth rate (CAGR) of 44.8% [1]. Metamaterials have attracted increasing interest from researchers over the past few decades due to their engineered ability to manipulate effective permittivity and/or permeability [2]. Studies have shown that electromagnetic waves interacting with metamaterials — including double-positive ($\varepsilon_r > 1$, $\mu_{eff} > 1$), negative-index (NRI), or zero-index (ZIM) media — exhibit distinctive refractive effects at the interface, such as normal or enhanced refraction [3–5]. In particular, antenna prototypes incorporating metamaterials have experimentally demonstrated improved and controlled radiation pattern response, including enhanced gain and beam shaping [6–8]. Overall, metamaterials have been found to be extremely effective in enhancing different metrics of interest for a diverse set of applications, including satellite communication, biosensing, and emerging wireless technologies such as 6G networks [7–10].

Patch antennas (PAs) are known for their planar structure and ease of integration. They have long been at the center of wireless communication systems delivering a high-quality connection in a compact space. As 6G and other high-frequency technologies emerge, PAs are increasingly expected to deliver higher gains and broader bandwidths while maintaining compactness and a high gain-bandwidth product (GBWP) [11, 12]. Although PAs are compact, there is a need to increase their gain without enlarging the aperture size. In addition, wideband (WB) characteristics are essential for modern communication systems, particularly in 6G, which demands high data rates and increased spectral efficiency. Hence, 6G communication systems require a high gain-bandwidth product (GBWP). Traditionally, GBWP is enhanced by manipulating the physical dimensions of the radiating patch, material properties of the substrate, and/or thickness of the substrate [13, 14]. However, an antenna with an electrically large form factor is unsuitable for compact, high-frequency 6G devices. Therefore, there is a growing need for non-traditional techniques to enhance the GBWP of a PA while being compact and efficient. One such technique is the use of metamaterials.

Metamaterials offer a transformative solution to enhance PA's GBWP by introducing artificial electromagnetic properties [15]. Among metamaterials, split ring resonators (SRRs) constitute a subgroup that generates strong magnetic resonances through circulating currents in concentric metallic rings with gaps [16]. Khoutar et al. designed a circular SRR on top of a PA, where the refractive index of these structures is close to zero, and they concentrate the radiation energy of a PA to enhance gain [17]. Choudhary et al. designed a PA with a complementary SRR and rectangular slots, presented with a superstrate [18]. Lakshmana et al. placed an SRR structure at a height of half the wavelength above an antenna array [19]. Saha et al. designed four rectangular complementary SRRs on a patch antenna and a layer of square SRRs on top of the antenna [20]. While the designs proposed in [17–23] demonstrated an average gain enhancement of 4 dBi, they exhibit some level of loss or attenuation, reduce the overall antenna efficiency, and restrict their capacity to enhance the antenna's GBWP to specific

* Corresponding author: Al-Moatasem Al-Hinaai (aawvp@mail.umkc.edu).

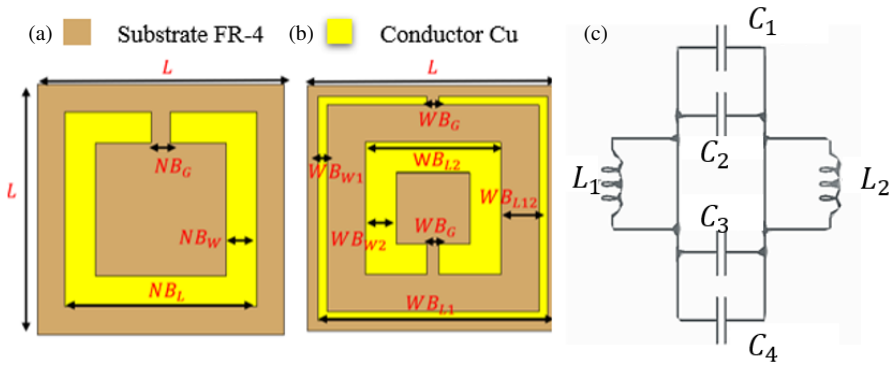

FIGURE 1. Unit-cell designs: (a) conventional MSRR, (b) proposed MSRR, and (c) equivalent circuit model. $C1$–$C4$ denote coupling/ring capacitances; $L1$–$L2$ denote inner/outer ring inductances.

SRR resonances. Metasurfaces have been reported in [24–26] for efficient cross-polarization conversion (CPC) for both normally and obliquely incident waves over ultra-wideband. However, their complex design and fabrication challenges make them impractical for GBWP improvement. Moreover, the narrowband (NB) effective permeability (μ_{eff}) of the metasurface presented in [24–26] limits their ability to enhance the gain over a wide frequency range. In contrast, our approach focuses on enhancing the μ_{eff}, which directly contributes to increasing the magnetic field across the bandwidth, increasing GBWP.

Traditional SRRs are limited by their narrowband resonance, which restricts their ability to enhance an antenna's GBWP beyond specific frequency ranges [27]. The modified split-ring resonator (MSRR) exhibits positive μ_{eff} and permittivity at its resonance frequency, enabling stronger magnetic coupling than conventional SRRs [28]. The MSRR exhibits a stronger coupling of the magnetic field than the SRR, enabling more efficient power transfer, and has a wideband PA application [11].

The novelty of this work lies in developing a wideband MSRR and integrating it with a PA, demonstrating close to 1 GHz of bandwidth and 2×–3× improvement in gain, yielding a high GBWP value relative to other existing designs. The study analyzes how the geometric parameters of the MSRR influence its μ_{eff} and, consequently, the instantaneous bandwidth (IBW) of the antenna system, establishing a direct connection between structural design, electromagnetic response, and transmission characteristics. A comprehensive simulation approach using Computer Simulation Technology (CST) Studio Suite was employed to design and optimize the MSRR rings. Prototypes of the optimized MSRR designs were then fabricated on an FR-4 material, and measured and compared against simulation data for S-parameter response, realized gain, and GBWP.

2. CHARACTERISTICS OF SRR RESONANCE

SRR unit-cell, a fundamental component in metamaterial design, exhibits unique electromagnetic properties primarily driven by its magnetic resonance [29]. The permeability $\mu(\omega)$ plays a key role in enhancing the magnetic response, allowing efficient interaction with the electromagnetic waves [30]. SRR consists of concentric metallic rings and gaps that induce circulating currents when being subjected to an external magnetic field, creating a magnetic dipole moment and enabling resonance at specific frequencies.

Double SRRs, comprising two concentric rings, offer enhanced capacitance and reduced electric dipole interference compared to single SRRs. In single SRRs, the charge accumulation near the gap induces an electric dipole moment that weakens the magnetic dipole. Conversely, in double SRRs, the opposing electric dipole moments cancel each other, resulting in stronger magnetic resonance and enhanced metamaterial performance. Each ring within the unit cell exhibits a distinct resonance frequency determined by its geometric dimensions. Consequently, a single (SRR) has one resonance, while a double SRR configuration introduces two resonances, and additional rings further expand the resonance spectrum.

A dual-resonance SRR unit cell, consisting of two concentric rings, supports distinct resonance frequencies (f_{inner} and f_{outer}), which are determined by the inductance (L) and capacitance (C) of each ring [31–33]:

$$f_{\text{inner}} = \frac{1}{2\pi\sqrt{L_{\text{inner}}C_{\text{inner}}}}, \quad f_{\text{outer}} = \frac{1}{2\pi\sqrt{L_{\text{outer}}C_{\text{outer}}}} \tag{1}$$

The outer ring resonates at a lower frequency due to its larger dimensions, while the inner ring resonates at a higher frequency. The dual resonances broaden the unit-cell's effective IBW and enhances electromagnetic interactions. The total impedance of the MSRR is given by:

$$Z_T = j\omega L\left(1-\omega^2 LC\right)^{-1} \tag{2}$$

where L is the total inductance, and C is the total capacitance. Eq. (2) shows how inductance and capacitance contributions from both rings which result in two distinct resonance frequencies.

3. RESULTS AND DISCUSSION

3.1. Simulation Analysis

The first step is to set up the outer ring based on Eqs. (1) and (2) by calculating the capacitance and inductance to achieve resonance around 8 GHz as shown in Fig. 1(a). Next, we add the

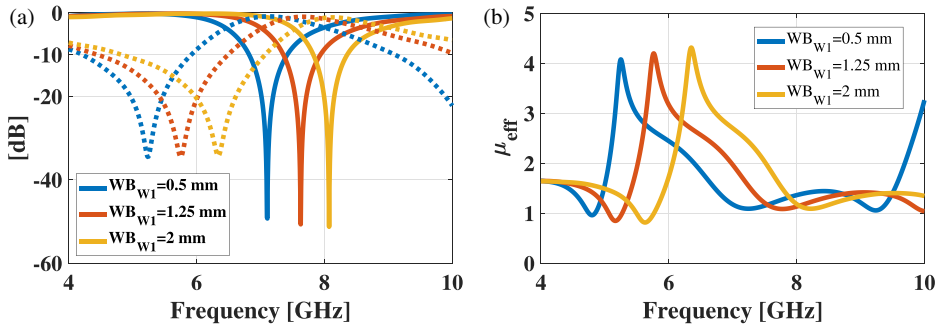

FIGURE 2. Comparison of a unit cell design with dual traces on one side, $WB_{W1} = WB_{W2}$ is adjusted by 0.5 mm: (a) S_{11} and S_{21}, shown as solid and dotted lines respectively, (b) effective permeability (μ_{eff}).

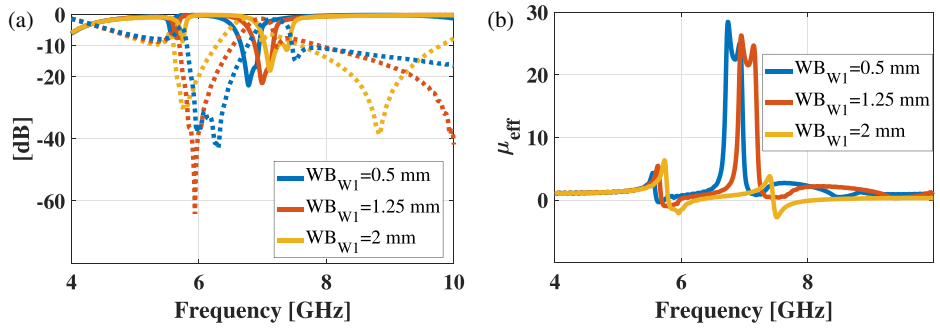

FIGURE 3. Comparison of a unit cell design with two traces on both sides rotated 180 degrees in phase, $WB_{W1} = WB_{W2}$ is adjusted by 0.5 mm: (a) S_{11} and S_{21}, shown as solid and dotted lines respectively, (b) effective permeability (μ_{eff}).

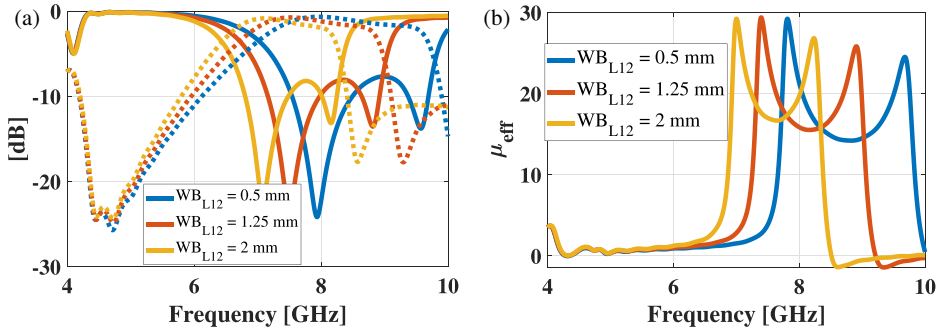

FIGURE 4. Comparison of a unit cell design with two traces on both sides rotated 180 degrees in phase, WB_{L12} is adjusted by 0.5 mm while WB_{W2} kept fixed at 0.3 mm: (a) S_{11} and S_{21}, shown as solid and dotted lines respectively, (b) effective permeability (μ_{eff}).

inner ring and vary the trace width until both rings exhibit interference and coupled resonance with their equivalent circuit (Figs. 1(b) and (c)). The design process focused on optimizing the dual-resonance MSRR unit cell to achieve a wideband resonance frequency of 8 GHz. Figs. 2(a) and 2(b) show the unit cell, S_{11}, and μ_{eff} responses for the initial design. The narrow resonance at 8 GHz, limited by low μ_{eff} restricts transmission bandwidth. Changes in gap size and trace width shift the resonance frequency.

To broaden the IBW, a backside trace was added and rotated 180 degrees. The change created a dual-resonance mechanism that broadened the operational bandwidth, as seen in Figs. 3(a) and 3(b), while maintaining strong coupling at both resonant frequencies. The IBW enhancement was achieved through asymmetry in ring widths, as depicted in Figs. 4(a) and 4(b), where inner and outer rings resonate at distinct frequencies.

Each adjustment in the MSRR parameters affects the electric and magnetic field distribution. The final design achieved a balance between inductive and capacitive elements, enabling wider IBW and stronger coupling for wideband applications.

The genetic algorithm (GA) approach yielded optimal values for inductance and capacitance to achieve dual resonances, achieving a 1 GHz IBW at the desired resonance frequency of 8 GHz. The MSRR parameters are: $P_W = 43.37$ mm, $P_L = 35.94$ mm, $G_W = 80$ mm, $G_L = 80$ mm, $Pin_N = 40$ mm, $Pin_S = 40$ mm, $Pin_W = 34$ mm, $Pin_E = 36$ mm, $L = 10$ mm, $NB_G = 0.5$ mm, $NB_W = 3$ mm, $NB_L = 6.8$ mm, $WB_{W1} = 0.4$ mm, $WB_{W2} = 1.35$ mm, $WB_{L2} = 6.2$ mm, $WB_G = 0.5$ mm, $WB_{L1} = 8.2$ mm, and $WB_{L12} = 1$ mm.

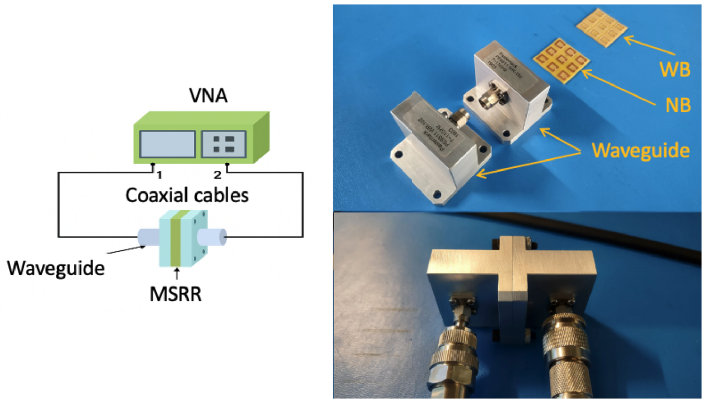

FIGURE 5. Waveguide measurement setup: the left-hand side shows the schematic connection, while the right-hand side shows a photograph of MSRR samples positioned between the two waveguides.

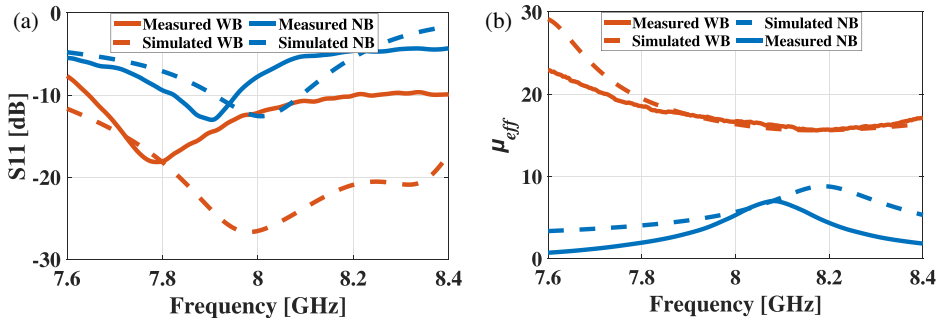

FIGURE 6. A simulation and measurement comparison of: (a) S_{11} and (b) effective permeability of MSRR (μ_{eff}).

The goal was to test the WB versus NB capability for improving PA GBWP. The antenna radiates frequencies from 7.6 to 8.4 GHz.

3.2. Waveguides Measurements

The waveguide-based measurement method is used to characterize the MSRR magnetic resonance, and a calibrated experimental setup was implemented, consisting of transmitting and receiving waveguides, a vector network analyzer (VNA), and a sample holder. The metamaterial sample, featuring specific geometric characteristics conducive to magnetic resonance, is placed between transmitting and receiving waveguides as shown in Fig. 5. VNA is utilized to sweep through the frequency range of 4 GHz–10 GHz, capturing scattering parameters (S-parameters) during the process using the through, reflect, line (TRL) calibration technique.

The reflection coefficient (S_{11}) plot, which reveals distinctive features associated with reflection linked to the magnetic response, is analyzed. Key equations used in this analysis include [34]:

$$S_{11}^{\text{MUT}} = \frac{[T_{11} - L_{11}]}{[M_{11} - L_{11}]}(-1) \tag{3}$$

$$S_{21}^{\text{MUT}} = \frac{[T_{21}]}{[L_{21}]}e^{-j\beta_0 d} \tag{4}$$

Equations (3) and (4) represent the reflection and transmission coefficients for the material under test (MUT), respectively, where T_{11}, L_{11}, M_{11}, T_{21}, and L_{21} are scattering parameters associated with the metamaterial and reference components. Specifically, L represents the scattering parameters of air, T the through scattering parameters, and M a metal composite panel MCP (reflect). The term β_0 is the plane wave propagation constant of the dominant TE_{10} mode in the empty waveguide, and d is the thickness of the MSRR [34]. The magnetic resonance is identified from features in the S_{11} plot, revealing insights into the material's magnetic properties. The effective permeability (μ_{eff}) of the MSRR is given by [35]:

$$\mu_{eff}(\omega) = \frac{2}{\sqrt{\frac{\omega}{c}} \times d} \times \frac{1 - (S_{21} - S_{11})}{1 + (S_{21} - S_{11})} \tag{5}$$

where d is the thickness of the MSRR, $\omega = 2\pi f$, and c is the speed of light.

The MSRR (μ_{eff}) can be affected by its design parameters. By optimizing the dimensions of the rings and gaps, we can tailor the resonance frequency and the IBW of the MSRR to suit specific applications. The enhanced effective permeability introduced by the MSRR structure allows for the precise control over the electromagnetic response of the metamaterial.

The waveguide measurements of $|S_{11}|$ and (μ_{eff}) highlight the performance improvements and have been measured using two waveguides as shown in Fig. 5. Fig. 6(a) presents the reflection coefficient $|S_{11}|$ results, where the wideband (WB) configuration maintains values below the -10 dB threshold over an IBW of 1 GHz, demonstrating effective impedance

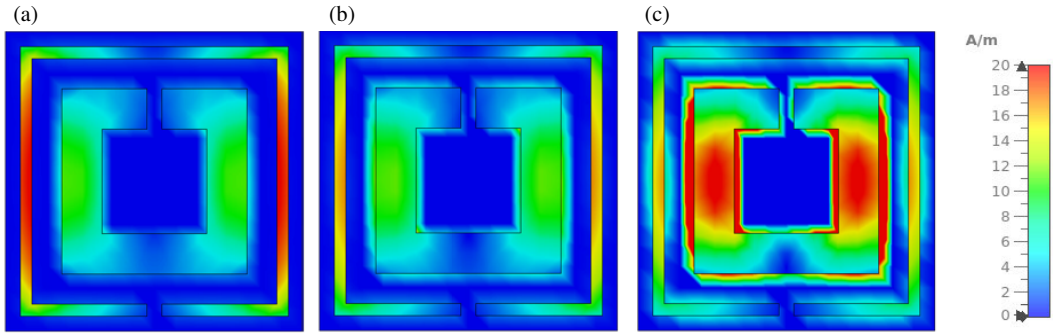

FIGURE 7. Unit cell MSRR surface current: (a) first resonance, (b) between the first and second resonances, (c) second resonance.

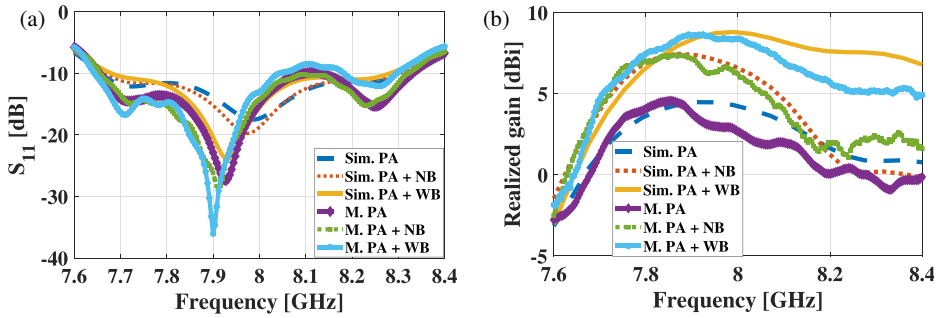

FIGURE 8. Comparison of simulation and measurement results for (a) $|S_{11}|$ and (b) realized gain of the PA.

matching and resonance. The narrowband (NB) configuration also exhibits resonance but over a narrower frequency range. While the measured results align well with the simulations, slight discrepancies are observed. Specifically, the measured resonance dips are shifted by less than 200 MHz from the simulated values, which can be attributed to fabrication tolerances and alignment factors during measurement. The permeability μ_{eff}, shown in Fig. 6(b), was derived using Eqs. (3), (4), and (5). The WB configuration exhibits higher μ_{eff} peaks than the NB configuration, signifying a stronger magnetic response over a broader frequency range. This enhanced permeability directly contributes to the improved resonance and extended IBW observed in the WB configuration. Differences between the simulated and measured μ_{eff} curves are evident, particularly in peak magnitude and sharpness. These deviations likely result from slight inconsistencies in material properties. The magnetic field alignment facilitated by the MSRR strengthens the electromagnetic properties of the antenna, enabling higher realized gain and wider IBW without compromising impedance matching.

It should be noted that the MSRR unit cell at 8 GHz is not deeply subwavelength, and therefore, the extracted effective permeability does not represent a unique bulk material parameter in the strict homogenization sense. Instead, the retrieved μ_{eff} should be interpreted as an effective response parameter of a finite periodic MSRR structure under TE_{10} waveguide excitation, inherently dependent on the excitation polarization and boundary conditions. Nevertheless, since both the narrowband and wideband MSRRs are characterized using identical waveguide fixtures, excitation modes, and retrieval procedures, the extracted μ_{eff} provides a consistent and meaningful metric for comparative evaluation of their magnetic response strength and operational bandwidth.

Figure 7 illustrates the surface current density distribution of the MSRR unit cell at representative frequencies. In Fig. 7(a), the current is primarily concentrated along the outer ring, indicating a dominant low-frequency magnetic resonance. In Fig. 7(b), the increased coupling between the inner and outer rings is observed, corresponding to the interaction region between the two resonances. Finally, Fig. 7(c) shows strong and localized current confinement on both rings, confirming cooperative dual-resonance behavior that underpins the wideband response of the proposed MSRR.

3.3. Reflection Coefficient $|S_{11}|$

The simulated and measured $|S_{11}|$ for the PA, with and without the MSRR, remain below the -10 dB threshold across a wide bandwidth, indicating effective impedance matching (see Fig. 8(a)). Without the MSRR, $|S_{11}|$ shows a single resonance dip at 8 GHz, corresponding to the inherent matching condition of the patch antenna. The addition of the MSRR, especially the WB MSRR, improves the $|S_{11}|$ profile by broadening the resonance. The NB MSRR sharpens impedance matching at a narrow resonance frequency, limiting IBW, while the WB MSRR broadens the resonance due to dual-resonance mechanisms, improving impedance matching and reducing losses.

3.4. Far-Field Realized Gain

Figure 8(b) compares the simulated and measured realized gains of the patch antenna with and without the proposed MSRR. The WB MSRR achieves a peak realized gain of 5–6 dBi across the 7.6–8.4 GHz band, representing an improvement of about 6 dBi compared to the standalone PA. In contrast, the NB MSRR enhances the gain only near its resonance and

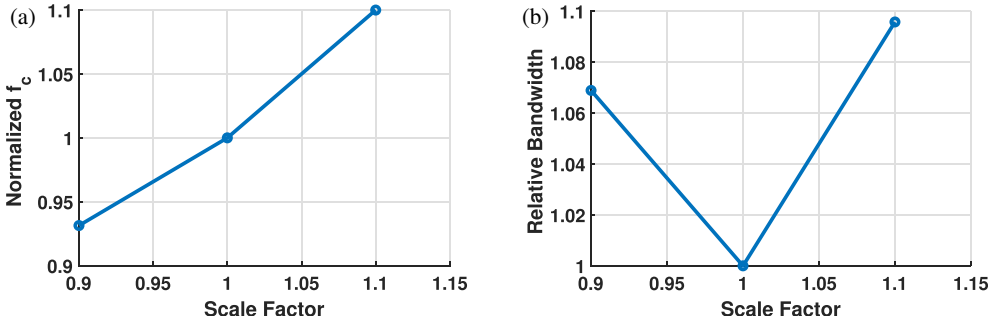

FIGURE 9. Effect of geometric scaling on MSRR performance: (a) normalized center frequency as a function of scale factor, (b) relative bandwidth as a function of scale factor.

TABLE 1. Comparison between proposed work and other SRR-based patch antenna designs.

Method	f_c [GHz]	Gain [dBi]	BW [%]	GBWP	Aperture [λ_c]
[17] 2018	3.75	3.17	5.8	145.70	1.41
[18] 2021	10.00	2.5	6.0	42.48	0.34
[19] 2018	9.00	1.0	7.7	74.57	0.75
[20] 2021	13.00	2.0	3.8	34.66	0.40
[22] 2025	4.50	∼3.0	∼12.0	<100	0.20
This Work	8.00	6.0	12.5	292.38	1.59

fails to maintain high performance across the full band. These results confirm that the proposed MSRR significantly enhances both peak gain and bandwidth, thereby validating the 3× improvement in transmission bandwidth over conventional SRRs. The reported 3× bandwidth refers to the −10 dB transmission impedance bandwidth of the proposed wideband MSRR unit cell, compared with a baseline double-ring SRR of the same footprint, fabricated on the same FR-4 substrate and tuned to the same center frequency (8 GHz). Table 1 demonstrates that the proposed MSRR-based patch antenna significantly outperforms previously reported designs in terms of gain-bandwidth product (GBWP) [17–20, 22]. Whereas earlier implementations exhibit restricted gain and narrow operational bandwidth, the proposed structure achieves a measured gain of 6 dBi together with a fractional bandwidth of 12.5%, yielding a GBWP of 292.38, the highest among the compared designs. These results validate the effectiveness of the MSRR-based configuration in simultaneously enhancing both gain and bandwidth without increasing the electrical aperture, highlighting its suitability for compact high-performance antenna applications.

3.5. Scalability and Fabrication Tolerance

To evaluate the scalability and fabrication tolerance of the proposed MSRR, a parametric study was conducted by uniformly scaling the lateral dimensions of the resonator while maintaining a fixed substrate thickness and material properties. Fig. 9(a) shows the normalized center frequency as a function of the scale factor, where a near-linear trend is observed. This behavior confirms that the MSRR resonance frequency scales predictably with geometry, indicating robustness against moderate dimensional variations and suitability for frequency translation to other operating bands.

Figure 9(b) presents the relative bandwidth normalized to the nominal design. The results indicate that the bandwidth remains nearly constant across the considered scaling range, demonstrating that the wideband response is preserved under geometric scaling. It confirms that the proposed dual-resonance MSRR architecture maintains its wideband characteristics despite dimensional variations, supporting its applicability to higher-frequency implementations and practical fabrication tolerances.

4. CONCLUSION

The study successfully overcomes the narrowband limitations of conventional SRRs by introducing an optimized wideband MSRR structure. The proposed MSRR expands the operating IBW to three times that of traditional SRRs, achieving a close to 1 GHz IBW and a peak gain improvement of 6 dBi when being integrated with a patch antenna. The optimization process, incorporating precise dimensional tuning and a genetic algorithm, highlights the role of dual-resonance mechanisms in enhancing IBW. The increased μ_{eff} of the MSRR improves magnetic coupling, impedance matching, and reduces reflection losses, making it highly effective for wideband antenna applications. The findings have broad implications for 6G wireless networks, remote sensing, satellite communications, and medical imaging, where high gain and wideband performance are crucial. Additionally, the MSRR's adaptability enables integration with various antenna types, extending its applicability across electromagnetic systems. Future research could explore higher-frequency optimizations, multi-band operation, and adaptive designs to further expand its technological impact.

REFERENCES

[1] Salgarkar, R., "Metamaterials market worth $1,387 million by 2029," *MarketsandMarkets*, Report, Available: https://www.prnewswire.com/news-releases/metamaterial-market-worth-1-38-billion-by-2029---exclusive-report-by-marketsandmarkets-302298490.html, 2024.

[2] Singh, A. K., M. P. Abegaonkar, and S. K. Koul, "A negative index metamaterial lens for antenna gain enhancement," in *2017 International Symposium on Antennas and Propagation (ISAP)*, 1–2, Phuket, Thailand, 2017.

[3] Zhou, H., Z. Pei, S. Qu, S. Zhang, J. Wang, Q. Li, and Z. Xu, "A planar zero-index metamaterial for directive emission," *Journal of Electromagnetic Waves and Applications*, Vol. 23, No. 7, 953–962, 2009.

[4] Ali, W. A. E., H. A. Mohamed, A. A. Ibrahim, and M. Z. M. Hamdalla, "Gain improvement of tunable band-notched UWB antenna using metamaterial lens for high speed wireless communications," *Microsystem Technologies*, Vol. 25, No. 11, 4111–4117, 2019.

[5] Hamad, E. K. I., W. A. E. Ali, M. Z. M. Hamdalla, and M. A. Bassiuny, "High gain triple band microstrip antenna based on metamaterial super lens for wireless communication applications," in *2018 International Conference on Innovative Trends in Computer Engineering (ITCE)*, 197–204, Aswan, Egypt, 2018.

[6] Enoch, S., G. Tayeb, P. Sabouroux, N. Guérin, and P. Vincent, "A metamaterial for directive emission," *Physical Review Letters*, Vol. 89, No. 21, 213902, 2002.

[7] Islam, M. R., B. Bais, M. Samsuzzaman, M. Z. Mahmud, H. Arshad, N. M. Sahar, and M. S. J. Singh, "G loaded complementary split square ring resonator-based SNG metamaterial for Wi-Fi, IoT & satellite applications," in *2021 7th International Conference on Space Science and Communication (IconSpace)*, 313–317, Selangor, Malaysia, 2021.

[8] Alam, M. J., M. R. I. Faruque, T. Allen, S. Abdullah, M. T. Islam, K. N. A. Maulud, and E. Ahamed, "Depiction and analysis of a modified theta shaped double negative metamaterial for satellite application," *Open Physics*, Vol. 16, No. 1, 839–847, 2018.

[9] Ali, W. A. E. and M. Z. M. Hamdalla, "Compact triple band-stop filter using novel epsilon-shaped metamaterial with lumped capacitor," *Journal of Instrumentation*, Vol. 13, No. 4, P04007, 2018.

[10] Azim, R., M. T. Islam, J. S. Mandeep, and A. T. Mobashsher, "A planar circular ring ultra-wideband antenna with dual band-notched characteristics," *Journal of Electromagnetic Waves and Applications*, Vol. 26, No. 14-15, 2022–2032, 2012.

[11] Kumar, P., T. Ali, and M. M. M. Pai, "Electromagnetic metamaterials: A new paradigm of antenna design," *IEEE Access*, Vol. 9, 18 722–18 751, 2021.

[12] Chamkur, D. V. and C. R. Byrareddy, "4G shaped wide band patch antenna for wireless applications," in *2018 3rd International Conference on Communication and Electronics Systems (ICCES)*, 323–328, Coimbatore, India, 2018.

[13] Ruze, J., "Antenna tolerance theory — A review," *Proceedings of the IEEE*, Vol. 54, No. 4, 633–640, Apr. 1966.

[14] Zhang, X. and L. Zhu, "Gain-enhanced patch antenna without enlarged size via loading of slot and shorting pins," *IEEE Transactions on Antennas and Propagation*, Vol. 65, No. 11, 5702–5709, Nov. 2017.

[15] Smith, D. R., R. Liu, and T. J. Cui, *Metamaterials: Theory, Design, and Applications*, Springer US, 2010.

[16] Padilla, W. J. and R. D. Averitt, "Imaging with metamaterials," *Nature Reviews Physics*, Vol. 4, No. 2, 85–100, 2022.

[17] Khoutar, F. Z., M. Aznabet, and O. E. Mrabet, "Gain and directivity enhancement of a rectangular microstrip patch antenna using a single layer metamaterial superstrate," in *2018 6th International Conference on Multimedia Computing and Systems (ICMCS)*, 1–4, Rabat, Morocco, 2018.

[18] Choudhary, A. K., S. Barman, T. Moyra, A. Debnath, and A. Bhattacharjee, "Gain enhancement of dual-band microstrip-fed antenna with complementary split ring resonators and rectangular slots embedded in patch for wireless applications using metamaterial cell-based superstrate," in *2021 2nd International Conference on Range Technology (ICORT)*, 1–6, Chandipur, Balasore, India, 2021.

[19] Lakshmana, V. N., M. Satyanarayana, and S. P. Singh, "Performance study of rectangular microstrip patch antennas with split ring resonator structure," in *2018 2nd International Conference on I-SMAC (IoT in Social, Mobile, Analytics and Cloud)*, 336–340, Palladam, India, 2018.

[20] Saha, D., A. K. Choudhary, and T. Moyra, "Dual band microstrip patch antenna and its gain enhancement for X band and Ku band application using metamaterial," in *2021 7th International Conference on Signal Processing and Communication (ICSC)*, 48–52, Noida, India, 2021.

[21] Mishra, P., R. Komatineni, and K. D. Kulat, "Millimeter wave MPA using metamaterial-substrate antenna array for gain enhancement," in *2023 National Conference on Communications (NCC)*, 1–4, Guwahati, India, 2023.

[22] Abdelkarim, M., M. Bahrouni, and A. Gharsallah, "A compact triple band antenna based on multiple split-ring resonators for wireless applications," *Electronics*, Vol. 14, No. 11, 2271, 2025.

[23] Zerrouk, A., M. L. Tounsi, T. P. Vuong, N. Corrao, and M. C. E. Yagoub, "Miniaturized patch array antenna using CSRR structures for 5G millimeter-wave communication systems," *Electronics*, Vol. 14, No. 9, 1834, 2025.

[24] Gao, X., L. Y. He, S. J. Yin, C. H. Xue, G. F. Wang, X. M. Xie, H. Xiong, Q. Cheng, and T. J. Cui, "Ultra-wideband low-RCS circularly polarized antennas realized by bilayer polarization conversion metasurfaces and novel feeding networks," *IEEE Transactions on Antennas and Propagation*, Vol. 72, No. 2, 1959–1964, Feb. 2024.

[25] Barkal, Y., J. Zbitou, L. E. Abdellaoui, A. Oukaira, and M. Hefnawi, "Ultra-wideband cross-polarization conversion metamaterial unit cell stable to incident angles at C-band," in *2024 Mediterranean Smart Cities Conference (MSCC)*, 1–5, Martil-Tetuan, Morocco, 2024.

[26] Osman, M., J. Yousaf, E. Almajali, M. I. Hussein, S. S. Alja'afreh, A. Altaf, and M. Elahi, "Ultra wideband highly efficient cross polarization conversion metasurface for multi-band applications," in *2023 Advances in Science and Engineering Technology International Conferences (ASET)*, 1–4, Dubai, United Arab Emirates, 2023.

[27] Tamandani, A., J. Ahmadi-Shokouh, and S. Tavakoli, "Wideband planar split ring resonator based metamaterials," *Progress In Electromagnetics Research M*, Vol. 28, 115–128, 2013.

[28] Attia, H., L. Yousefi, M. M. Bait-Suwailam, M. S. Boybay, and O. M. Ramahi, "Enhanced-gain microstrip antenna using engineered magnetic superstrates," *IEEE Antennas and Wireless Propagation Letters*, Vol. 8, 1198–1201, 2009.

[29] Tan, C., Y. Wang, Z. Yan, X. Nie, Y. He, and W. Chen, "Superconducting filter based on split-ring resonator structures," *IEEE Transactions on Applied Superconductivity*, Vol. 29, No. 4, 1–4, 2019.

[30] Wang, Q., Y. Zhang, K. Fang, and Y. Li, "Magnetic polarizability of the metamaterials with negative permeability," in *2017*

1st International Conference on Electrical Materials and Power Equipment (ICEMPE), 33–35, Xi'an, China, 2017.

[31] Rajni, and A. Marwaha, "An accurate approach of mathematical modeling of SRR and SR for metamaterials," *Journal of Engineering Science & Technology Review*, Vol. 9, No. 6, 82–86, 2016.

[32] Lheurette, E., "Metamaterials for non-radiative microwave functions and antennas," *Metamaterials and Wave Control*, 67–86, 2013.

[33] Alibakhshikenari, M., B. S. Virdee, T. A. Elwi, I. D. Lubangakene, R. K. R. Jayanthi, A. A. Al-Behadili, Z. A. A. Hassain, S. M. Ali, G. Pau, P. Livreri, and S. Aïssa, "Design of a planar sensor based on split-ring resonators for non-invasive permittivity measurement," *Sensors*, Vol. 23, No. 11, 5306, 2023.

[34] Hassan, A. M., J. Obrzut, and E. J. Garboczi, "A Q-band free-space characterization of carbon nanotube composites," *IEEE Transactions on Microwave Theory and Techniques*, Vol. 64, No. 11, 3807–3819, Nov. 2016.

[35] Moniruzzaman, M., M. T. Islam, M. R. Islam, N. Misran, and M. Samsuzzaman, "Coupled ring split ring resonator (CR-SRR) based epsilon negative metamaterial for multiband wireless communications with high effective medium ratio," *Results in Physics*, Vol. 18, 103248, 2020.